Journal of Applied Polymer Science

Enhanced Piezoelectric Responses and Crystalline Arrangement of Electroactive Polyvinylidene Fluoride/Magnetite Nanocomposites

Zen-Wei Ouyang, Erh-Chiang Chen, Tzong-Ming Wu
Department of Materials Science and Engineering, National Chung Hsing University, Taichung, Taiwan 402, Republic of China
Correspondence to: T.-M. Wu (E-mail: tmwu@dragon.nchu.edu.tw)

ABSTRACT: The well distributed and electroactive polyvinylidene fluoride (PVDF)/magnetite nanocomposites were successfully fabricated using a mixed solvent system (THF/DMF). Dynamic mechanical properties of the fabricated PVDF/magnetite nanocomposites indicate significant enhancements in the storage modulus as compared with that of neat PVDF. By adding 2 wt % magnetite nanoparticles into the PVDF matrix, the thermal stability of nanocomposites could be enhanced about 26°C as compared with that of PVDF. The β-phase fraction of PVDF is significantly enhanced with increasing the voltage of electric field poling. The piezoelectric responses of PVDF/magnetite films are extensively increased about five times in magnitude with applied strength of electrical field at 35 MV/m. The change of piezoelectric responses during the applied electric field may be due to the relative long arrangement of PVDF units along the direction of electric field poling and thus increases the values of L_p^* and l_c. © 2014 Wiley Periodicals, Inc. J. Appl. Polym. Sci. **2014**, *131*, 40941.

KEYWORDS: composites; mechanical properties; morphology; X-ray

Received 4 March 2014; accepted 29 April 2014
DOI: 10.1002/app.40941

INTRODUCTION

Polyvinylidene fluoride (PVDF) has attracted more scientific and technological interest due to its excellent piezoelectric and ferroelectric properties.[1–4] PVDF is a semicrystalline polymer, which contains five different crystalline phases known as α, β, γ, δ, and ε phases.[5] The polymorphs that occur most frequently are the α and β crystalline phases. The thermodynamically stable α-phase consists of the antiparallel tgtg'-chain arrangement in the unit cell and thus has no net polarization. The α-phase is obtained directly cooling from the melt or by solvent cast at solvent evaporation temperatures above 120°C.[6–8] However, the β-phase shows a net nonzero dipole moment because of the parallel packing of all-trans chain in an orthorhombic unit cell. The electroactive β-phase can be achieved by stretching the α-phase at the temperature below 100°C or by casting from the strongly polar solvent at evaporation temperatures below 70°C.[9] Solvent evaporation at higher temperature causes a mixture of α- and β-phase, with the portion of α-phase increasing as the evaporation temperature increases. Electric field poling or drawing, a process of realignment of the dipoles in crystallite, is also used to convert the more readily obtained α- and γ-phases into the β-phase.[10–12] From above investigations, the structural conformation of PVDF is strongly dependent on the processing, thermal, or mechanical treatments that the polymer undergoes.

Recently, several approaches have also been made to attain the electroactive β-phase of PVDF, including the introduction of nanoparticles, such as ferrite, titanium oxide, and $BaTiO_3$, as well as the use of clay and hydrated ionic salt to prepare composite materials.[13–19] Polymer nanocomposites defined by the size of dispersed phase having at least one dimension <100 nm contain relatively high aspect ratio and draw much attention due to their outstanding physical, mechanical, and thermal properties. Compared with traditional polymer composites, nanocomposites show significant improvements at lower amount of inorganic fillers.[20] Due to the interfacial effects, the presence of nanoscale fillers in the polymer matrix causes noteworthy variations of charge distribution and transportation of the dielectric materials. Therefore, experimental incorporation of ferrite nanoparticles with magnetic characteristic into PVDF could significantly enhance both piezoelectric and magnetic properties for the fabricated nanocomposites.

The aim of this study is to obtain extremely high content of polar crystalline phase of PVDF/magnetite nanocomposites by adding 13 nm monodispersed magnetite nanoparticles and imposing electrical field poling. The monodispersed 13 nm magnetite nanoparticles were prepared using the thermal decomposition method. Various concentrations of magnetite nanoparticles were added into PVDF via solution mixing process in a mixed solvent system (THF/DMF) to obtain PVDF/

magnetite magnetoelectric nanocomposites. The samples were then poled with various applied strengths of electrical field. The structure and morphology of the poled PVDF/magnetite nanocomposites were characterized. Special attention is devoted to demonstrate the cooperative effect of electric poling-induced chain arrangement and adding nanoparticle on the formation of polar β crystalline phase of PVDF. Our goal has been to comprehensively study systematic changes in the structure and morphology of PVDF/magnetite nanocomposites and to relate these into subsequent piezoelectric behavior in an attempt to understand and utilize the piezoelectric phenomenon.

EXPERIMENTAL

Materials

PVDF ($M_w = 530{,}000$) was purchased from Aldrich. Iron acetylacetonate, 1, 2-hexadecanediol oleylamine, phenyl ether, and oleic acid were obtained from Acros and all used without further purification. Other reagents, including dimethylformide (DMF) and tetrahydrofuran (THF), were all analytical grade and used as received.

Synthesis of PVDF/Magnetite Nanocomposites

The monodispersed 13 nm magnetite nanoparticles were prepared using the thermal decomposition of a mixture of iron acetylacetonate, oleic acid, 1, 2-hexadecanediol oleylamine, and phenyl ether oleic acid were added into a three-necked bottle and purged with N_2 to inhibit the effect of oxygen. The mixture was then heated to reaction temperature at 300°C and kept at this temperature for the desired time. Then the mixture was precipitated with ethanol, centrifuged to remove the solvent, and redispersed into hexane.

The preparation of PVDF/magnetite nanocomposites was performed using a mixed solvent system (THF/DMF). Various amounts of PVDF and magnetite nanoparticle were individually dissolved or dispersed at 60°C in a mixed solvent at the THF/DMF ratio of 70/30. When PVDF and magnetite nanoparticle was dissolved or well dispersed, the two solutions were combined and mixed via sonication until the solutions were uniform. The fabricated PVDF/magnetite nanocomposite was then spread on glass substrate to evaporate the solvent at evaporation temperatures of 60°C and dried in vacuum at 60°C for 24 h. The thickness of cast film was about 0.035 mm.

Characterization of PVDF/Magnetite Nanocomposites

High-resolution transmission electron microscopy (HRTEM) performed on a Hitachi HF-2000 at 200 kV was used to characterize the structure and morphology of the magnetite and PVDF/magnetite nanocomposites. The averaged particle sizes of magnetite nanoparticles were determined from HRTEM images using Sigmascan Pro 5 software package. For PVDF/magnetite nanocomposites, HRTEM analysis were obtained using the droplet of PVDF/magnetite nanocomposites in solution on the surface of carbon-coated copper grid and then air-dried for 2 h. Two-dimensional (2D) wide-angle X-ray diffraction (WAXD) experiment equipped with Ni-filtered CuK_α radiation was recorded on a Bruker D8 Discover SSS with a two-dimensional Vantec-2000 area detector, which is a xenon-based gaseous avalanche detector with an active area of 14 × 14 cm^2 (2048 × 2048 $pixel^2$) with a spatial resolution of 68 μm^2 on the area detector. The sample to detector distance is 7 cm and the diffraction angle resolution is 0.02° with a collection time of 600 s. One-dimensional (1D) WAXD profiles were obtained by integrating the corresponding 2D WAXD images. Small-angle X-ray scattering (SAXS) measurements were performed using a Bruker D8 Discover equipped with Ni-filtered CuK_α radiation in the transmission mode. The sample to detector distance was ~30 cm and the scattering vector (q, nm^{-1}) is defined as $q = 4\pi(\sin\theta)/\lambda$, where λ and 2θ are the wavelength and the scattering angle, respectively.

The thermal behaviors of PVDF/magnetite nanocomposites were carried out using a Perkin Elmer TG/DTA 6300 thermoanalyzer in a temperature range of 25–1000°C at 10°C /min heating rate under nitrogen atmosphere. The storage modulus (E') of the PVDF/magnetite nanocomposites was obtained on a Perkin Elmer DMA 7e dynamic mechanical analyzer (DMA). All samples were investigated in a temperature range of −90 to 120°C at 5°C/min heating rate and 5 Hz constant frequency. The piezoelectric properties were measured using a d_{33} piezoelectric coefficient meter (model YE2730A).[21,22] All specimens were coated with a thin layer of Ag on both sides. For electric field poling experiments, the samples were incubated in silicon oil bath using the self-design assembly for the poling treatment. After 1 h of electric field poling at 60°C with various applied electric fields, the piezoelectric response (d_{33}) of the poling sample was analyzed. The data shown here represented the mean measurement values from at least three samples. Maximum electric field to obtain the reasonable experimental data was 35 MV/m. By applying the electric field larger than 35 MV/m, several defects, such as pinhole or porosity, will observe on the surface of test samples. This might induce the electric crossover during the measurement.

RESULTS AND DISCUSSIONS

Characterization and Morphology of PVDF/Magnetite Nanocomposites

Figure 1 presents the HRTEM images of monodispersed 13 nm magnetite synthesized using the thermal decomposition method. From this result, it can be seen that the distribution of particle size is extremely uniform and the average diameter of magnetite particle is about 13 nm. The X-ray diffraction pattern of magnetite also inset in Figure 1 reveals six strong diffraction peaks at $2\theta = 30.2$, 35.5, 43.2, 53.5, 57.1, and 62.9°, corresponding to (220), (311), (400), (422), (511), and (440) crystalline planes of magnetite phase, respectively.[23,24] Both HRTEM and XRD results demonstrate the 13 nm magnetite nanoparticles containing extremely uniform distribution were successfully fabricated using thermal decomposition method. According to previous investigation, the dispersed nanoparticles could cause the polymer to swell when the radius of the nanoparticles was less than the radius of gyration, R_g, of the polymer.[25] The R_g of PVDF calculated on the basis of the freely jointed chain model is 24 nm, which is greater than the radius of synthesized magnetite nanoparticles. By adding the nanoparticles into the PVDF matrix, the polymer chain could swell to increase its radius of gyration. This increase in R_g could provide more free volume

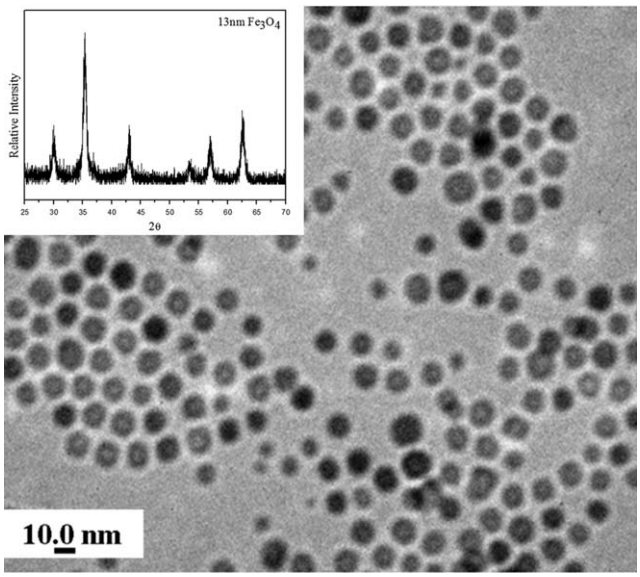

Figure 1. HRTEM images of monodispersed 13 nm magnetite nanoparticles (inset the X-ray diffraction pattern of magnetite nanoparticles).

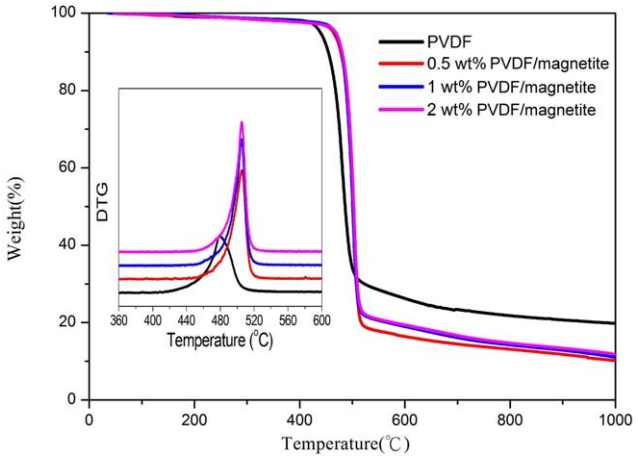

Figure 3. TGA thermograms of PVDF and PVDF/magnetite composites (inset is the derivative thermogravimetric (DTG) curve of PVDF and PVDF/magnetite composites with different loading of magnetite). [Color figure can be viewed in the online issue, which is available at wileyonlinelibrary.com.]

for PVDF polymer chain to transform into its more extended β crystalline form during the fabrication of PVDF/magnetite nanocomposites. At the same time, the electrostatic charge of magnetite nanoparticles obtained using zeta potential analysis exhibited negative surface charge (−12.0 mV) at pH∼6, which is also favored for the formation of β-phase of PVDF.[8,26] From above data, the incorporation of 13 nm magnetite with negative surface charge into PVDF matrix could expect to gain more β-phase of PVDF. This result is similar to previous investigation reported by Goncalves et al.[14] To confirm the structure of fabricated PVDF/magnetite composites, Figure 2 shows the HRTEM images of the PVDF/magnetite composites with various loadings of magnetite. From these data, the magnetite nanoparticles are well distributed in PVDF matrix and the amount of magnetite increases with increasing the loadings of magnetite. These results suggest that the PVDF/magnetite nanocomposites containing extremely distributed nanoparticles have been successfully synthesized.

Thermal, Mechanical, and Piezoelectric Properties of PVDF/Magnetite Nanocomposites

To better understand the effect of magnetite nanoparticle on the thermal stability of PVDF matrix, TGA analysis was performed to investigate the thermal behavior of PVDF and PVDF/magnetite nanocomposites. Figure 3 presents the curves of weight loss versus temperature of PVDF and PVDF/magnetite nanocomposites at a heating rate of 10°C /min. Although all experimental results of PVDF and PVDF/magnetite nanocomposites have almost the same shape, PVDF/magnetite nanocomposites seem to be more stable if we compare its TGA curve with the curve of pure PVDF matrix in the temperature range of 420–520°C. The temperature corresponding to maximum degradation rate (T_{max}) was determined by the peak position of derivative thermogravimetric curve. Evidently, the T_{max} of the PVDF/magnetite nanocomposites prepared with various contents of magnetite is higher than that of pure PVDF matrix. The T_{max} of PVDF is 479.1°C and significantly increases to 505.0, 505.4, and 505.6°C for the magnetite loading of 0.5, 1, and 2 wt %, respectively. The incorporation of magnetite nanoparticles enhanced thermal stability about 26°C as compared with that of PVDF. This result demonstrates that the addition of magnetite nanoparticles in PVDF caused better thermal stability and thus T_{max} obviously shifted to higher temperatures. This phenomenon may be due to the inorganic nature of magnetite with well distributed structure, which provided the better hindrance of heat sources, thus improved the thermal stability. However, the values of T_{max} were slightly increased with increasing the loadings of magnetite. This result is probably due to the presence of oleic acid on

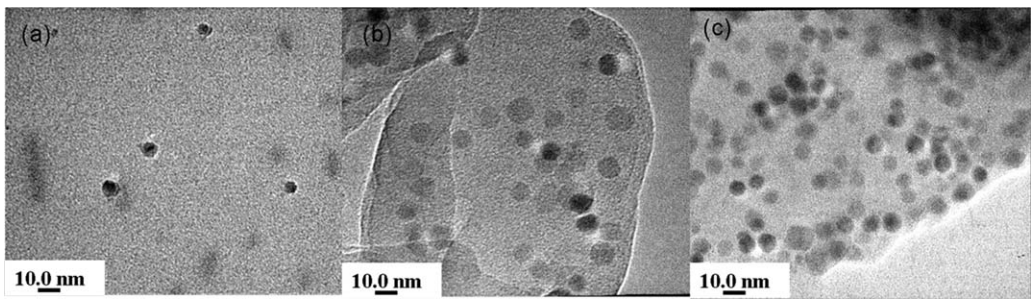

Figure 2. HRTEM image of the (a) 0.5 wt %, (b) 1wt %, and (c) 2 wt % PVDF/magnetite composites.

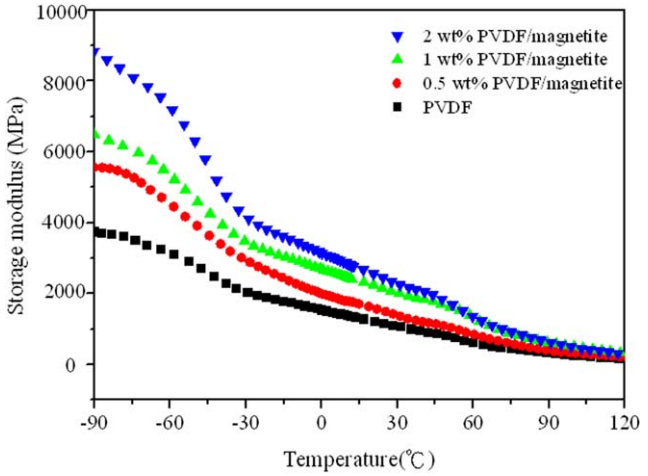

Figure 4. Storage modulus (E') as a function of temperature of PVDF and PVDF/magnetite nanocomposites. [Color figure can be viewed in the online issue, which is available at wileyonlinelibrary.com.]

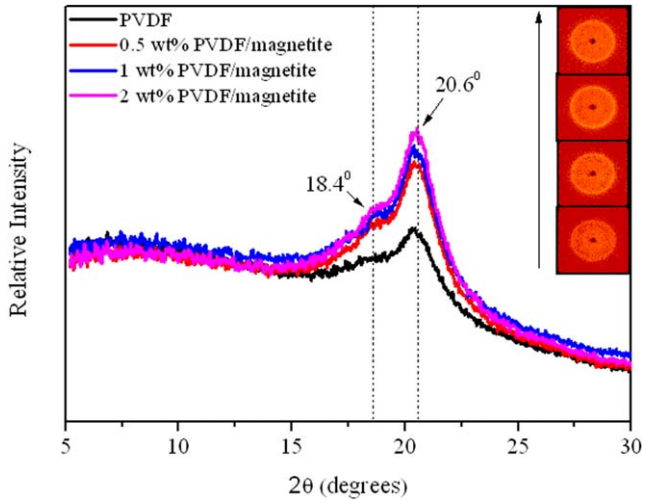

Figure 5. 1D WAXD patterns of PVDF and PVDF/magnetite nanocomposites (inset is 2D WAXD image of PVDF and PVDF/magnetite composites in the order from top (2 wt % PVDF/magnetite nanocomposites) to bottom (PVDF) with decreasing loading of magnetite). [Color figure can be viewed in the online issue, which is available at wileyonlinelibrary.com.]

the surface of magnetite, which will cause certain weight loss below the temperature of 420°C thus limit the further enhancement of thermal stability of nanocomposites.

DMA analysis was operated to investigate the storage modulus (E') of PVDF/magnetite nanocomposites. The E' versus temperature for neat PVDF and its corresponding nanocomposites are illustrated in Figure 4. It is clear that the addition of magnetite nanoparticles could significantly enhance the E' of PVDF over the whole temperature range. Moreover, the values of E' of the composites increased with increasing the contents of magnetite. For example, when −90°C was selected as a point for comparison, the values of E' for pure PVDF and its composites with magnetite loading of 0.5, 1, and 2 wt % were determined as 3760, 5562, 6494, and 8839 *MPa*, respectively. In particular, when the magnetite loading was 2 wt %, the value of E' at −90°C was ~135% higher than that of pure PVDF. The remarkable increase of the storage modulus at the lower temperature range may be due to the reinforcement effect of the addition of inorganic and stiff magnetite nanoparticle as well as the well distributed structure of nanocomposites, leading to the remarkable improvement on the stiffness of PVDF matrix. From above results, the significant improvements in thermal and mechanical properties of PVDF/magnetite nanocomposites have successfully achieved.

For the piezoelectric properties, our aim was intended to comprehensively study the change of β-phase and piezoelectric coefficient d_{33} for PVDF/magnetite films using various strengths of electric field and related these into the subsequent changes in the structure and morphology of the fabricated PVDF/magnetite nanocomposites. According to previous investigations,[18,27] FTIR instrument was usually used to determine the ratio of β-phase for the fabricated materials. Two major absorption peaks at 764 and 840 cm^{-1} can be attributed to the CF_2 bending/skeletal CF—CH—CF bending and CH_2 rocking, which were identified qualitatively and quantitatively to the α- and β-phase for PVDF, respectively.[27] For the experiments of electric field poling, the samples were incubated in silicon oil bath. The absorption bands of silicon oil were overlapped with the absorption peaks at 764 and 840 cm^{-1}. Therefore, FTIR spectrum can't be well distinguished the data of PVDF and silicon oil. In this study, wide-angle X-ray diffraction (WAXD), a power tool to determine the polymorphic composition in crystallizable polymer, is selected to identify the ratio of β-phase for PVDF and its composites. Figure 5 shows one-dimensional (1D) WAXD pattern for PVDF and PVDF/magnetite nanocomposites. This data was obtained by integrating the corresponding two-dimensional (2D) WAXD images also inset in this figure. From this experimental result, it can be clear seen that all samples exhibit one intense diffraction peak at $2\theta = 20.6°$ corresponding to the (200/110) reflection of β-phase for PVDF.[28] There is a small

Table I. The Calculated β-Phase Fraction of Pure PVDF and PVDF/Magnetite Nanocomposites with Various Strengths of Electric Field

Calculated β-phase fraction (%)							
Electrical field poling	0 (Mv/m)	7 (Mv/m)	14 (Mv/m)	21 (Mv/m)	28 (Mv/m)	35 (Mv/m)	42 (Mv/m)
PVDF 0.5 wt % PVDF/magnetite	17.3 ± 0.2	23.6 ± 0.3	23.9 ± 0.3	24.5 ± 0.3	28.7 ± 0.3	30.3 ± 0.4	29.4 ± 0.3
	17.8 ± 0.2	24.1 ± 0.3	25.0 ± 0.3	26.8 ± 0.3	30.8 ± 0.4	32.2 ± 0.4	29.4 ± 0.3
1 wt % PVDF/magnetite	18.4 ± 0.2	25.2 ± 0.3	25.7 ± 0.3	27.7 ± 0.3	31.7 ± 0.4	33.5 ± 0.4	30.6 ± 0.4
2 wt % PVDF/magnetite	19.2 ± 0.3	26.3 ± 0.3	26.5 ± 0.3	28.4 ± 0.3	36.3 ± 0.4	36.5 ± 0.4	32.9 ± 0.4

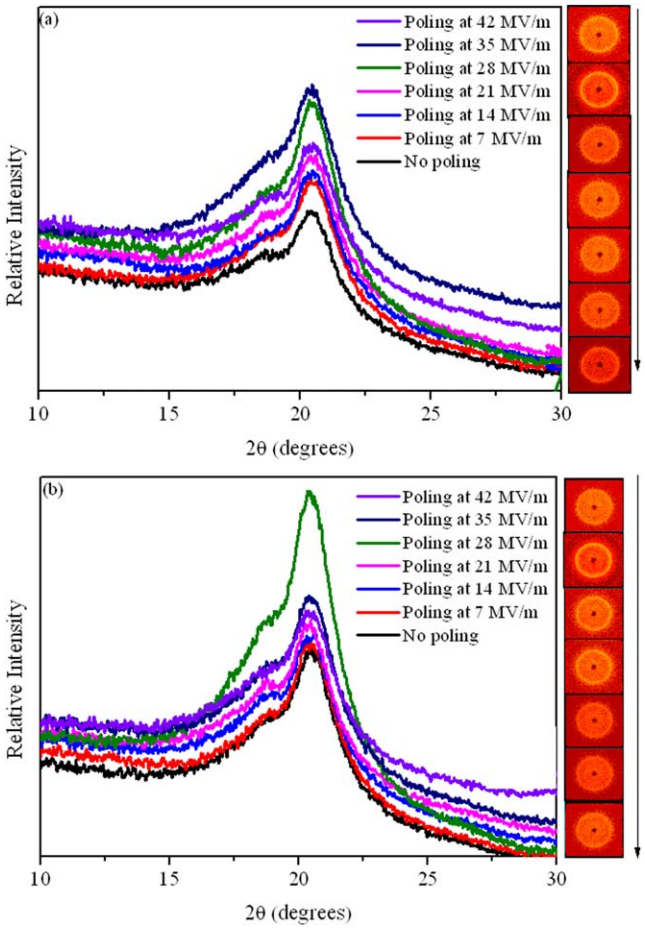

Figure 6. 1D WAXD pattern of (a) 0.5 wt % PVDF/magnetite and (b) 2 wt % PVDF/magnetite nanocomposites with various strengths of electric field. 2D WAXD images of corresponding PVDF/magnetite composites in the order from bottom (no electric field poling) to top (poling at 42 MV/m) with increasing voltage of electric field poling were also inserted in this figure. [Color figure can be viewed in the online issue, which is available at wileyonlinelibrary.com.]

trace of reflection observed at $2\theta = 18.4°$ corresponding to the (020) reflection of α-phase. Upon nanoparticle addition, the peak at 18.4° slightly increases in intensity, indicating a small increase in the α-phase content of the composites. However, the increase in intensity of diffraction peak at 20.6° for PVDF/magnetite nanocomposites is relatively higher than that of pure PVDF, suggesting a considerable increase in the β-phase content of the composites. The actual contents of α- and β-phase were directly calculated by the α- and β-crystallinity from the peak-fitting results in Figure 5. Because the peak intensity of α-phase is very small and very close to the intensity of amorphous background, the fitting data is almost meaningless. Therefore, the calculated β-phase fraction was summarized in Table I. It can be seen that the β-phase fraction of PVDF is slightly increased with increasing the loadings of magnetite nanoparticles. The piezoelectricity of PVDF, 0.5 wt % PVDF/magnetite, 1 wt % PVDF/magnetite and 2 wt % PVDF/magnetite nanocomposites determined using a d_{33} piezoelectric coefficient meter were 7.3, 7.3, 7.6, and 7.8 pC/N, respectively. The obtained piezoelectric coefficients were in good agreement with the one reported from Inoue et al. for similar preparation method.[29] The value of d_{33} was slightly increased with the incorporation of the magnetite nanoparticles. From these results, the addition of magnetite nanoparticle into PVDF increased the β-phase fraction of PVDF as well as their piezoelectricity.

According to previous investigations,[10–12,30] electric field poling can be used to convert the obtained α-phases into the β-phase. To obtain the optimum condition of piezoelectric PVDF/magnetite film, we investigated the effect of electric field poling (E_p) on the change of β-phase fraction and the coefficient of piezoelectric (d_{33}). The E_p was determined by dividing the electrodes distance (d) into high voltage (V). 1D WAXD patterns obtained by integrating the corresponding 2D WAXD images for 0.5 wt % PVDF/magnetite and 2 wt % PVDF/magnetite nanocomposites with various electric fields were shown in Figure 6. From these results, the intensity of diffraction peak at $2\theta = 20.6°$ was increased with increasing the strength of electric field to 35 MV/m. By applying the strength of electric field larger than 35 MV/m, the intensity of diffraction peak slightly decreased due to the possible structural defect of electric crossover through the PVDF/magnetite film. Similar results were also obtained for PVDF and 1 wt % PVDF/magnetite nanocomposites. The calculated β-phase fractions of PVDF and PVDF/magnetite nanocomposites with various strengths of electric fields were summarized in Table I. The β-phase fraction of PVDF is significantly enhanced with increasing the voltage of electric field poling. For the PVDF/magnetite nanocomposites, the content of β-phase showed a cooperative effect of electric field poling and nanoparticle on the formation of polar β-phase in PVDF. The piezoelectricity of PVDF and PVDF/magnetite nanocomposites with various strengths of applied electric field were listed in Table II. Below the strength of electric field of 35 MV/m, all data indicated that the value of d_{33} increased as the strength of electric field increased. For example, when electric field poling at 35 MV/m was selected as a point for comparison, the values of d_{33} for poling samples are about five times in magnitude

Table II. The Coefficient of Pizeoelectirc Response (d_{33}) of PVDF and PVDF/Magnetite Nanocomposites with Various Strengths of Electric Field

d_{33} (pC/N)							
Electrical field poling	0 (Mv/m)	7 (Mv/m)	14 (Mv/m)	21 (Mv/m)	28 (Mv/m)	35 (Mv/m)	42 (Mv/m)
PVDF 0.5 wt % PVDF/magnetite	7.3 ± 0.1	14.3 ± 0.2	14.6 ± 0.2	19.2 ± 0.2	31.4 ± 0.4	33.4 ± 0.4	31.6 ± 0.4
	7.3 ± 0.1	15.4 ± 0.2	18.8 ± 0.2	21.0 ± 0.2	35.3 ± 0.4	35.9 ± 0.4	32.1 ± 0.4
1 wt % PVDF/magnetite	7.6 ± 0.1	16.2 ± 0.2	22.4 ± 0.2	24.5 ± 0.3	36.7 ± 0.4	37.6 ± 0.4	34.5 ± 0.4
2 wt % PVDF/magnetite	7.8 ± 0.1	17.4 ± 0.2	26.4 ± 0.2	28.2 ± 0.3	39.8 ± 0.5	40.6 ± 0.5	35.8 ± 0.4

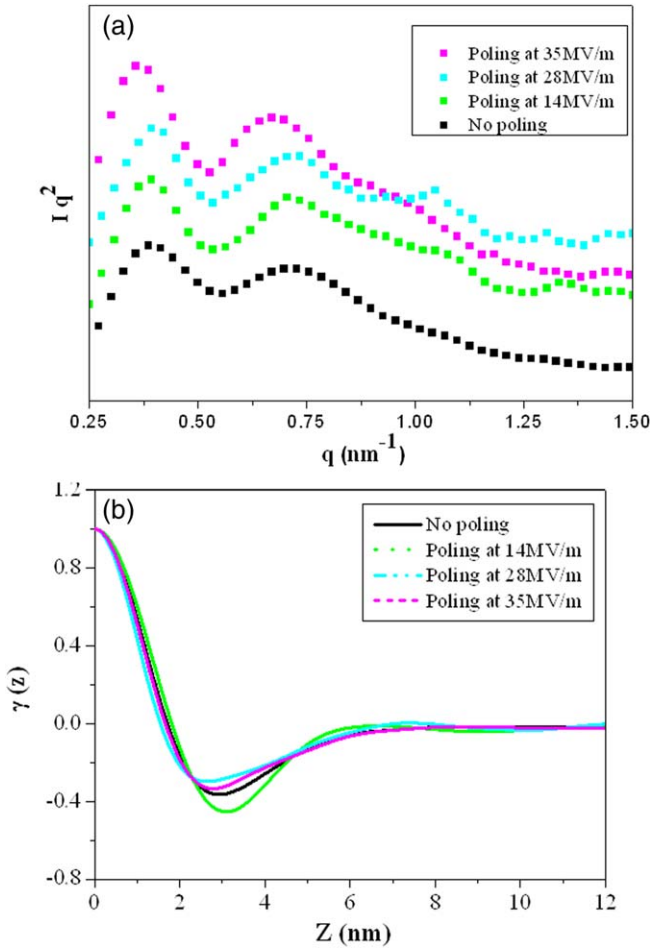

Figure 7. (a) Lorentz-corrected SAXS intensity profiles as a function of the strength of electric field for pure PVDF. (b) One-dimensional correlation function calculated from the SAXS profiles for pure PVDF at various strengths of electric field. [Color figure can be viewed in the online issue, which is available at wileyonlinelibrary.com.]

higher than the samples without electric field poling. For the same experimental condition of electric field poling, the d_{33} value of nanocomposites was higher than the data of pure PVDF matrix, which might be attributed to the addition of 13 nm of magnetite nanoparticles.

The above findings suggest that the microstructure of PVDF/magnetite nanocomposites is strongly affected by the strength of electric field. Therefore it is very important to understand the effect of electric field poling on the molecular chain arrangement of PVDF/magnetite nanocomposites. SAXS technique is frequently used to study the microstructure of materials. Figure 7(a) shows the Lorentz-corrected SAXS profiles of 2 wt % PVDF/magnetite nanocomposites treated at various strengths of electric field. To estimate the long period (L_p^*) and crystal layer thickness (l_c) of the PVDF/magnetite nanocomposites with various strengths of electric field, the scattering data were analyzed according to the pseudo-two-phase model using a one-dimensional correlation function which can be taken directly as the Fourier transform of the scattering intensity.[31,32] The normalized one-dimensional correlation function is defined as $r(z)=\frac{1}{Q}\int_0^\infty q^2 I(q)\cos(qz)dq$, where Q is a scattering invariant. Figure 7(b) shows a typical one-dimensional correlation function as a function of the magnitude of the depths z for the specimens. The L_p^* and l_c ($l_c = L_p^* - l_a$) of the PVDF/magnetite nanocomposites calculated from above data are listed in Tables III and IV. The L_p^* value for pure PVDF and its composites with magnetite loading of 0.5, 1, and 2 wt % were determined as 5.74, 6.05, 6.10, and 6.21 nm, respectively. The value of l_c was also increased with the addition of magnetite nanoparticles. These results indicated that the incorporation of magnetite nanoparticles can enhance the regular chain arrangement of PVDF. The L_p^* value of PVDF significantly increased from 5.74 to 6.59 nm as the strength of electric field increased to 35 MV/m. In the meantime, the l_c value was simultaneously increased with increasing strength of electric field. During the applied

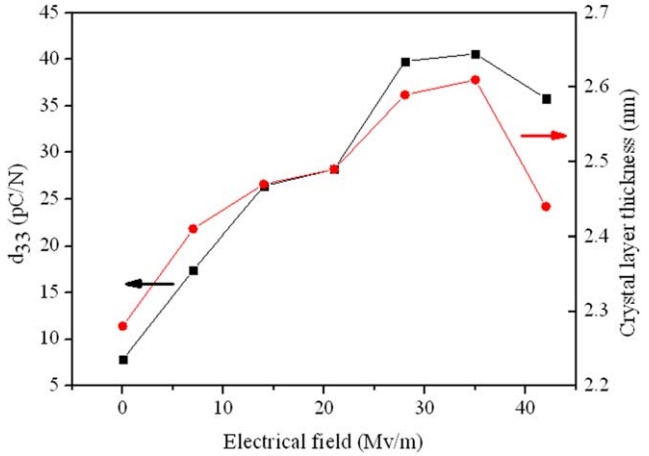

Figure 8. Plots of d_{33} and crystal layer thickness as a function of the strength of electric field for 2 wt % PVDF/magnetite nanocomposites. [Color figure can be viewed in the online issue, which is available at wileyonlinelibrary.com.]

Table III. Long Period (L_p^*) and Crystal Layer Thickness (l_c) Obtained from One-Dimensional Correlation Function of PVDF and PVDF/Magnetite Nanocomposites with Various Strengths of Electric Field

Long period (L_p^*; nm)							
Electrical field poling	0 (Mv/m)	7 (Mv/m)	14 (Mv/m)	21 (Mv/m)	28 (Mv/m)	35 (Mv/m)	42 (Mv/m)
PVDF 0.5 wt % PVDF/magnetite	5.74	5.96	6.47	6.53	6.54	6.59	6.62
	6.05	6.19	6.51	6.55	6.56	6.88	6.75
1 wt % PVDF/magnetite	6.10	6.26	6.60	6.77	7.02	7.11	6.88
2 wt % PVDF/magnetite	6.21	6.29	6.67	6.85	7.08	7.20	7.00

Table IV. Crystal Layer Thickness (l_c) Obtained from One-Dimensional Correlation Function of PVDF and PVDF/Magnetite Nanocomposites with Various Strengths of Electric Field

Crystal layer thickness (l_c) (nm)							
Electrical field poling	0 (Mv/m)	7 (Mv/m)	14 (Mv/m)	21 (Mv/m)	28 (Mv/m)	35 (Mv/m)	42 (Mv/m)
PVDF 0.5 wt % PVDF/magnetite	1.93	2.21	2.23	2.27	2.27	2.33	2.30
	2.16	2.23	2.27	2.30	2.32	2.37	2.19
1 wt % PVDF/magnetite	2.20	2.37	2.41	2.44	2.51	2.53	2.27
2 wt % PVDF/magnetite	2.28	2.41	2.47	2.49	2.59	2.61	2.44

electric field, relative long sequence of PVDF units may be arranged along the direction of electric field poling and thus increases the values of L_p^* and l_c. Similar tendency obtained for PVDF/magnetite nanocomposites was also listed in Tables III and IV.

Figure 8 shows the plots of d_{33} and crystal layer thickness versus the strength of electric field for 2 wt % PVDF/magnetite nanocomposites. Similar tendency was also obtained for PVDF, 0.5 and 1 wt % PVDF/magnetite nanocomposites. From above results, they demonstrate that the change of the piezoelectric behavior and molecular structure of PVDF and PVDF/magnetite nanocomposites were strongly dominated by the strength of electric field. Both data increased as the strength of electric field increased to 35 MV/m. By applying the strength of electric field larger than 35 MV/m, both data slightly decreased. This might be due to the higher strength of electric field to induce the structure defect during the measurement.

CONCLUSIONS

The well distributed and electroactive PVDF/magnetite nanocomposites were successfully fabricated using a mixed solvent system (THF/DMF). Mechanical properties of the fabricated 2 wt % PVDF/magnetite nanocomposites show significant enhancements in the storage modulus (8839 MPa) when compared with that of neat PVDF (3760 MPa). The remarkable increase of the storage modulus at the lower temperature range may be attributed to the reinforcement effect of the presence of rigid magnetite nanoparticle as well as the well distributed structure of nanocomposites, leading to the prominent improvement on the stiffness of the PVDF matrix. The incorporation of 2 wt % magnetite nanoparticles into the PVDF matrix enhanced thermal stability about 26°C as compared to that of PVDF. The piezoelectric responses of PVDF/magnetite nanocomposites were extensively increased about five times in magnitude with applied strength of electrical field at 35 MV/m. The change of piezoelectric responses during the applied electric field may be due to the relative long arrangement of PVDF units along the direction of electric field poling and thus increases the values of L_p^* and l_c.

ACKNOWLEDGMENTS

The financial support provided by National Science Council through the project NSC99-2212-E-005-012-MY3 is greatly appreciated.

REFERENCES

1. Martins, P.; Lanceros-Méndez, S. *Adv. Funct. Mater.* **2013**, *23*, 3371.
2. Yee W. A.; Kotaki, M.; Liu, Y.; Lu, X. H. *Polymer* **2007**, *48*, 512.
3. Wang, M.; Shi, J. H.; Pramoda, K. P.; Goh, S. H. *Nanotechnology* **2007**, *18*, 235,701.
4. Martins, P.; Lopes, A. C.; Lanceros-Méndez, S. *Prog. Polym. Sci.* **2014**, *39*, 683.
5. Salimi, A.; Yousefi, A. A. *J. Polym. Sci. Part B: Polym. Phys.* **2004**, *42*, 3487.
6. Lovinger, A. J. *Science* **1983**, *220*, 1115.
7. Sencadas, V.; Gregorio Filho, R.; Lanceros-Mendez, S. *J. Non-Cryst. Solid* **2006**, *352*, 2226.
8. Botelho, G.; Lanceros-Mendez, S.; Goncalves, A. M.; Sencadas, V.; Rocha, J. G. *J. Non-Cryst. Solid* **2008**, *354*, 72.
9. Nalwa, H. S. Ferroelectric Polymers: Chemistry, Physics and Applications; Marcel Dekker Inc.: New York, **1995**, p 63.
10. Tashiro, K.; Takano, K.; Kobayashi, M.; Chatani, Y.; Tadokoro, H. *Polymer* **1983**, *24*, 199.
11. Darestani, M. T.; Coster, H. G. L.; Chilcott, T. C.; Fleming, S.; Nagarajan, V.; An, H. *J. Membr. Sci.* **2013**, *434*, 184.
12. Coster, H. G. L.; Darestani, M. T.; Chilcott, T. C. *Desalination* **2011**, *283*, 52.
13. Mendes, S.; Costa, C.; Caparros, C.; Sencadas, V.; Lanceros-Méndez, S. *J. Mater. Sci.* **2012**, *47*, 1378.
14. Goncalves, R.; Martins, P. M.; Caparros C.; Martins, P.; Benelmekki, M.; Botelho, G.; Lanceros-Mendez, S.; Lasheras A.; Gutierrez, J.; Barandiaran J. M. *J. Non-Cryst. Solid* **2013**, *361*, 93.
15. Patro, T. U.; Mhalgi, M. V.; Khakhar, D. V.; Misra, A. *Polymer* **2008**, *49*, 3486.
16. Lund, A.; Gustafsson, C.; Bertilsson, H.; Rychwalski, R. W. *Compos. Sci. Technol.* **2011**, *71*, 222.
17. An, N. L.; Liu, H. Z.; Ding, Y. C.; Zhang, M.; Tang, Y. P. *Appl. Surf. Sci.* **2011**, *257*, 3831.
18. Martins, P.; Costa, C. M.; Lanceros-Mendez, S. *Appl. Phys. A: Mater. Sci. Process* **2011**, *103*, 233.
19. He, L.; Sun, J.; Wang, X.; Wang, C.; Song, R.; Hao, Y. *Polym. Int.* **2013**, *62*, 638.
20. Pavlidou, S.; Papaspyrides, C. D. *Prog. Polym. Sci.* **2008**, *33*, 1119.

21. Lidmila, E. J. B. *J. Eur. Ceram. Soc.* **2011**, *21*, 1413.

22. Izyumskaya, N.; Alivov, Y. I.; Cho, S. J.; Morkoccedil, H.; Lee, H.; Kang, Y. S. *Crit. Rev. Solid State Mater. Sci.* **2007**, *32*, 111.

23. Tombs, N. C.; Rooksby, H. P. *Acta Crtstallogr.* **1951**, *4*, 474.

24. JCPDS card 03-065-3107 (Joint Committee on Powder Diffraction Standard, Swarthmore).

25. Mackay, M. E.; Tuteja, A.; Duxbury, P. M.; Hawker, C. J.; Van Horn, B.; Guan, Z.; Chen, G.; Krishnan, R. S.; *Science* **2006**, *311*, 1740.

26. Andrew, I. S.; Clarke, D. R. *Langmuir* **2008**, *24*, 8435.

27. Sencadas, V.; Gregorio, R.; Lanceros-Mendez, S. *J. Macromol. Sci. B: Phys.* **2009**, *48*, 514.

28. Guan, F.; Wang, J.; Pan, J.; Wang, Q.; Zhu, L. *Macromolecules* **2010**, *43*, 6739.

29. Inoue, M.; Tada, Y.; Suganuma, K.; Ishiguro, H. *Polym. Degrad. Stab.* **2007**, *92*, 1833.

30. Gomes, J.; Nunes, J. S.; Sencadas, V.; Lanceros-Mendez, S. *Smart Mater. Struct.* **2010**, *19*, 65010.

31. Strobl, G. R. The Physics of Polymers. Springer: New York, **1997**.

32. Barbi, V.; Funari, S. S.; Gehrke, R.; Scharnagl, N.; Stribeck, N. *Macromolecules* **2003**, *36*, 749.